J. Fluid Mech. (2010), *vol.* 659, *pp.* 505–515.
doi:10.1017/S0022112010003101

On the retrograde propagation of critical thermal convection in a slowly rotating spherical shell

SHIN-ICHI TAKEHIRO†

Research Institute for Mathematical Sciences, Kyoto University, Sakyo-ku, Kyoto 606-8502, Japan

(Received 27 January 2010; revised 1 June 2010; accepted 4 June 2010;
first published online 16 July 2010)

The retrograde propagation mechanism of critical thermal convection with a sectorial pattern emerging in a slowly rotating spherical shell is investigated through vorticity budget analysis. In the equatorial region, stretching and shrinking of the fluid columns in the direction of the axis of rotation due to the radial component of velocity causes retrograde propagation, whereas in the mid-latitudes, tilting of the radial component of planetary vorticity by the radial shear of the latitudinal component of velocity is dominant. The switching of the propagating direction from retrograde to prograde according to the increase in the rotation speed of the shell originates from the transition of the morphology of vortices from the 'banana-shaped' type due to the constraint of the spherical geometry to the columnar type due to the Taylor–Proudman constraint. The variation of the morphology of vortices reverses the tendency of stretching/shrinking of fluid columns accompanied by their cylindrically radial displacement.

Key words: convection, rotating flows, vortex dynamics

1. Introduction

The problems associated with Boussinesq thermal convection in rotating spherical shells have been studied for approximately 50 years with respect to applications to the internal fluid motions of the celestial bodies (e.g. Chandrasekhar 1961; Roberts 1968; Busse 1970*a*, *b*). The set-up of the model is the simplest physical configuration including essential elementary processes of thermal convection in the stellar and planetary interiors. In particular, the primary focus has been on thermal convection in rapidly rotating shells relevant to geophysical applications due to the smallness of the diffusivities of the fluid constituent. Based on the recent developments in computational facilities, the characteristics of critical thermal convection in rapidly rotating spheres and spherical shells have been widely realized. Numerical studies by Zhang & Busse (1987) and Zhang (1992) have revealed that the emergence of local two-dimensional Taylor columns elongated in the direction of the axis of rotation, as revealed by the pioneering study of Busse (1970*b*), occurs in a limited range of Prandtl numbers. Taylor columns locally emerge when the Prandtl number is larger than $O(1)$ (columnar convection), whereas when the Prandtl number is equal to or less than $O(1)$, Taylor columns do not localize, but rather extend spirally in

† Email address for correspondence: takepiro@gfd-dennou.org

the cylindrically radial direction (spiraling-columnar convection). When the Prandtl number is decreased further, an equatorially wall-attached structure appears as a critical mode (wall-attached convection). Based on these results, Busse's asymptotic theory has been re-examined (Yano 1992; Jones, Soward & Mussa 2000; Dormy *et al.* 2003), and physical interpretations of spiraling (Takehiro 2008) and wall-attached structures (Zhang 1993, 1994) have been presented.

The columnar and spiraling-columnar convection emerging in rapidly rotating shells propagates in the prograde direction. This characteristic originates from the topographic β effect (e.g. Busse 1986; Hirsching & Yano 1994; Takehiro 2008). On the other hand, the pattern of critical convection propagates in the retrograde direction when the rotation rate of the shell is sufficiently small. A pioneering study by Busse (1970*a*) expanded the governing equations by the small Coriolis parameter and showed the retrograde propagation from the first order of the expansion. Busse (1973) then revealed that their previous analysis was correct only in the limit of zero Prandtl number or for thin shells. The perturbation calculation in the limit of the small rotation rate was performed by Geiger & Busse (1981). They showed that the solution described by sectorial spherical harmonics Y_l^l appears as a critical mode, except for cases involving large Prandtl numbers and thick shells, and obtained an accurate expression of retrograde propagation frequency. Zhang & Busse (1987) performed numerical calculations of critical convection for the case of a radius ratio of 0.4 and found that the transition from retrograde to prograde propagation occurs around a Taylor number of $T = 10^4$ when the Prandtl number is larger than or equal to $O(1)$, whereas this transition occurs at a larger Taylor number when the Prandtl number is smaller than $O(1)$. Takehiro & Hayashi (1995) confirmed a similar transition of the propagation direction for various values of the radius ratio.

However, in contrast to the case of rapidly rotating spherical shells, there appears to be no satisfactory physical explanation of the retrograde propagation occurring in slowly rotating shells, although the asymptotic analytical expression of the solution is completely solved. For example, certain studies have interpreted the retrograde propagating solution as two-dimensional barotropic Rossby waves on a rotating sphere (e.g. Gilman 1975), but this interpretation is misleading because the vortex tubes of the critical convection in slowly rotating shells elongate along the spherical shell, and the radial component of vorticity is relatively small. The radial component of vorticity is proportional to the first-order magnitude of the square root of the Taylor number in the asymptotic expansion in the limit of a small rotation rate (Busse 1970*a*; Geiger & Busse 1981).

Therefore, in this paper, we intend to obtain a physical understanding of the retrograde propagation mechanism of critical convection in slowly rotating shells. The model of thermal convection in a rotating spherical shell and the numerical methods are described in § 2. In § 3, a typical structure of retrograde propagation critical convection in a slowly rotating shell is illustrated and compared with that of prograde propagating critical convection. In § 4, a budget analysis of the colatitudinal component of vorticity is performed. Section 5 summarizes the results.

2. Model

Let us consider a spherical shell with inner and outer radii r_i and r_o rotating with angular velocity Ω. The shell is filled with a Boussinesq fluid with thermal expansion coefficient α and kinematic and thermal diffusivities ν and κ, respectively. The gravitational force $-g_o \boldsymbol{r}/r_o$ is directed towards the centre of the shell, where $\boldsymbol{r}$ is

the position vector with respect to the centre of the shell, and g_o is the gravitational acceleration at the outer sphere of the shell. Not only the fluid but also the inner sphere contain a homogeneous heat source, and so the temperature gradient at the static state is given by $-\beta \boldsymbol{r}$. Linearized equations for disturbances with respect to the basic state with no motion and this temperature gradient are as follows:

$$E\left(\frac{\partial \boldsymbol{u}}{\partial t} - \nabla^2 \boldsymbol{u}\right) + 2\boldsymbol{k} \times \boldsymbol{u} + \nabla p = R\frac{\boldsymbol{r}}{r_o}\Theta, \tag{2.1}$$

$$\frac{\partial \Theta}{\partial t} - \boldsymbol{u} \cdot \boldsymbol{r} = \frac{1}{P}\nabla^2 \Theta, \tag{2.2}$$

$$\nabla \cdot \boldsymbol{u} = 0, \tag{2.3}$$

where $\boldsymbol{u}$ is the velocity, Θ is the temperature disturbance, p is the pressure and $\boldsymbol{k}$ is the unit vector in the direction of the axis of rotation. These equations are non-dimensionalized using the thickness of the shell $D = r_o - r_i$ as the length scale, the viscous diffusion time D^2/ν as the time scale, βD^2 as the temperature scale and $\rho\nu\Omega$ as the pressure scale, where ρ is the mean density of the fluid. The non-dimensional parameters appearing in the following equations:

$$R = \frac{\alpha g_o \beta D^3}{\nu\Omega}, \quad E = \frac{\nu}{\Omega D^2}, \quad P = \frac{\nu}{\kappa} \tag{2.4}$$

are the modified Rayleigh number, the Ekman number, and the Prandtl number, respectively. The boundary conditions are the impermeable, free-slip and fixed-temperature conditions:

$$\boldsymbol{r} \cdot \boldsymbol{u} = \frac{\partial}{\partial r}\left(\frac{\boldsymbol{u} \times \boldsymbol{r}}{r^2}\right) = \Theta = 0 \quad \text{at } r = \frac{\eta}{1-\eta}, \frac{1}{1-\eta}, \tag{2.5}$$

where $\eta = r_i/r_o$ is the ratio of the inner and outer radii.

We first obtain representative critical convection solutions for both slowly and rapidly rotating cases. The actual numerical calculations are performed using the equations described by the toroidal and poloidal potentials. The variables that appear in the equations are expanded with spherical harmonic functions in the horizontal direction and Chebyshev polynomials in the radial direction. This set of equations constitutes a linear eigenvalue problem for each azimuthal (longitudinal) wavenumber. Selecting the values of the Prandtl number, the Ekman number and the radius ratio, the neutral Rayleigh number giving zero growth rate for each azimuthal wavenumber is searched by solving the eigenvalue problem iteratively. We then find the critical Rayleigh number, the frequency, and the azimuthal wavenumber. The spherical harmonic functions and Chebyshev polynomials are calculated up to 40th latitudinal wavenumber and the 32nd degree, respectively.

For the cases of slow rotation rates, the values of the Ekman number, the Prandtl number and the radius ratio of the inner and outer radii are varied in the ranges of $E = 0.1$–10, $P = 10^{-2}$–10^2 and $\eta = 0.4$–0.8, respectively. The critical convection at $E = 10^{-2}$, $P = 1$ and $\eta = 0.4$ is also presented as a rapidly rotating case for comparison.

The validity of the programme is checked by comparing the numerical results with the analytic expression of the stress-free cases with $\eta = 0.2$ and 0.3 in Geiger & Busse (1981). The values of the Rayleigh number and the frequency coincided with each other to four and three significant digits, respectively, in the ranges of $E = 1$–10^2 and

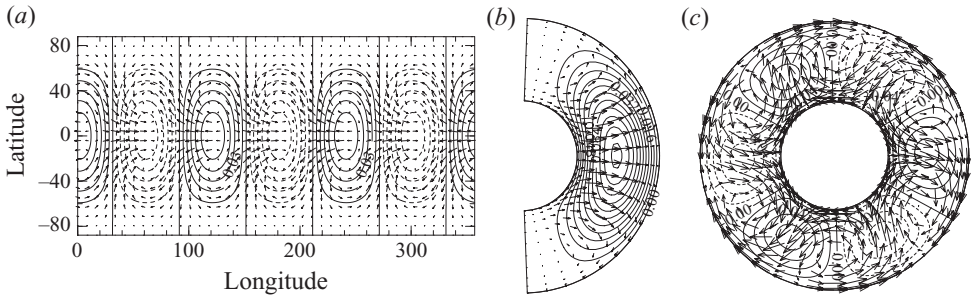

FIGURE 1. Typical structure of critical thermal convection in a slowly rotating spherical shell. $\eta = 0.4$, $E = 0.1$, $P = 1$ and $R = 114.854$. The pattern propagates in the retrograde direction with a frequency of 2.13544. (*a*) The temperature field (contours) at the middle of the shell ($r = 1.0$), and the velocity field (arrows) in the upper level ($r = 1.2$). (*b*) Meridional cross-section where the temperature field is maximum in the azimuthal direction. The contours and arrows indicate the temperature and velocity fields, respectively. (*c*) The equatorial cross-section. The contours and arrows indicate the temperature and velocity fields, respectively.

$P = 0.1$–10. Moreover, the critical Rayleigh number in the case of $E = 10^4$, $P = 1$ and $\eta = 0.4$ accurately converged to the value of the non-rotating case to four significant digits.

3. Critical modes of thermal convection

Figure 1 shows a representative structure of critical thermal convection for the case of slow rotation with the parameters of $\eta = 0.4$, $E = 0.1$, $P = 1$ and $R = 114.854$. The pattern propagates in the retrograde direction with a frequency of 2.13544. As described by Geiger & Busse (1981), the temperature and radial velocity fields consist of the sectorial spherical harmonic function Y_3^3 (figure 1*a*). The horizontal velocity field in an upper layer is converging on the equatorial minimum of the temperature field and is diverging from the equatorial maximum. A meridional cross-section reveals that the vortex tube is not elongated in the direction of the axis of rotation but bends along the spherical shell (figure 1*b*). Based on the equatorial cross-section, the vortex tubes have symmetric properties with respect to the longitudinal and radial directions, similar to the structure in no-rotation cases (figure 1*c*).

In contrast to figure 1, figure 2 illustrates a representative structure of critical thermal convection in the case of rapid rotation with the parameters of $\eta = 0.4$, $E = 10^{-2}$, $P = 1$ and $R = 31.5121$. The pattern propagates in the prograde direction with a frequency of 11.0877. The equatorially symmetric vortex pairs can be observed in the velocity field on a spherical surface, suggesting the existence of the Taylor-columnar structure (figure 2*a*). In a meridional cross-section, a vortex column elongated in the direction of the axis of rotation is distorted by the outer spherical surface (figure 2*b*). The vortex tubes observed in the equatorial cross-section tilt in the prograde-outward direction, which appears to be in the direction of the spiraling-columnar convection (figure 2*c*).

Figure 3 shows an overhead view of the vortex tubes described by the contour surfaces of the absolute value of vorticity. In a slowly rotating case, the vortex tubes bend along the spherical shell and constitute a banana-shaped structure. On the other hand, in a rapidly rotating case, vortex tubes are elongated in the direction of the axis of rotation, forming a Taylor-columnar structure.

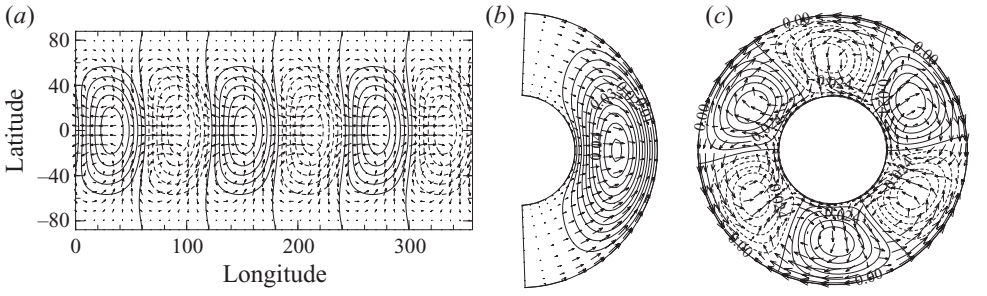

FIGURE 2. Typical structure of critical thermal convection in a rapidly rotating spherical shell. $\eta = 0.4$, $E = 10^{-2}$, $P = 1$ and $R = 31.5121$. The pattern propagates in the prograde direction with a frequency of 11.0877. (*a*) The temperature field (contours) at the middle of the shell ($r = 1.0$), and the velocity field (arrows) in the upper level ($r = 1.2$). (*b*) A meridional cross-section where the temperature field is maximum in the azimuthal direction. The contours and arrows indicate the temperature and velocity fields, respectively. (*c*) The equatorial cross-section. The contours and arrows indicate the temperature and velocity fields, respectively.

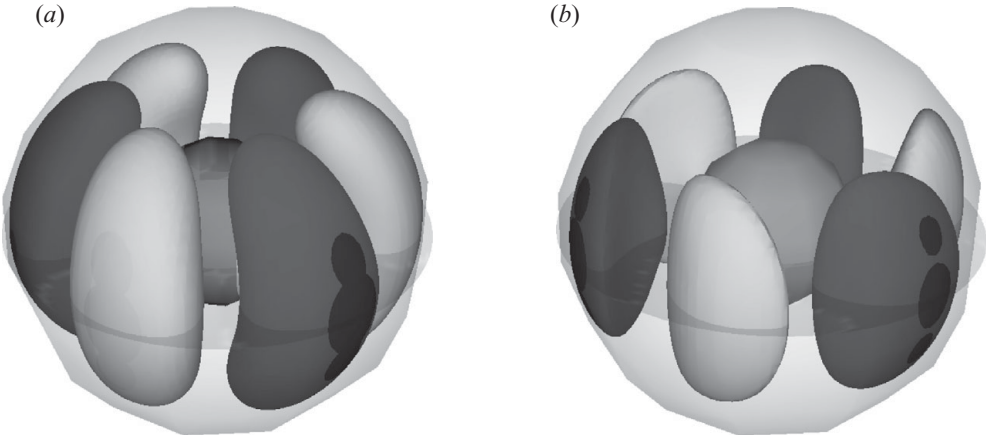

FIGURE 3. Comparison of the morphology of vortices between the cases with slow and rapid rotation rates. The contour surfaces of the absolute value of vorticity are observed obliquely from above. White and black surfaces indicate positive and negative colatitudinal components of vorticity, respectively. (*a*) The slow-rotation case (corresponding to figure 1). (*b*) The rapid-rotation case (corresponding to figure 2).

4. Budget analysis of the vorticity equation

In the previous section, we have observed that the vortex tubes of critical convection in the slowly rotating case bend along the spherical shell and elongate in the latitudinal direction. Therefore, it is appropriate to examine the colatitudinal component of vorticity in order to capture the physical properties of critical convection in a slowly rotating spherical shell. The equation for the time development of the colatitudinal component of vorticity is obtained by operating $\nabla\times$ to (2.1):

$$\frac{\partial \omega_\theta}{\partial t} = \frac{2}{E}\left(-\frac{\sin\theta}{r}\frac{\partial u_\theta}{\partial \theta} - \frac{u_r \sin\theta}{r} + \cos\theta\frac{\partial u_\theta}{\partial r}\right) + \frac{R}{E r_o}\frac{1}{\sin\theta}\frac{\partial \Theta}{\partial \phi} + \left[\nabla^2\omega_\theta - \frac{2\cos\theta}{r^2\sin\theta^2}\frac{\partial \omega_\phi}{\partial \phi} + \frac{2}{r^2}\frac{\partial \omega_r}{\partial \theta} - \frac{\omega_\theta}{r^2\sin^2\theta}\right], \quad (4.1)$$

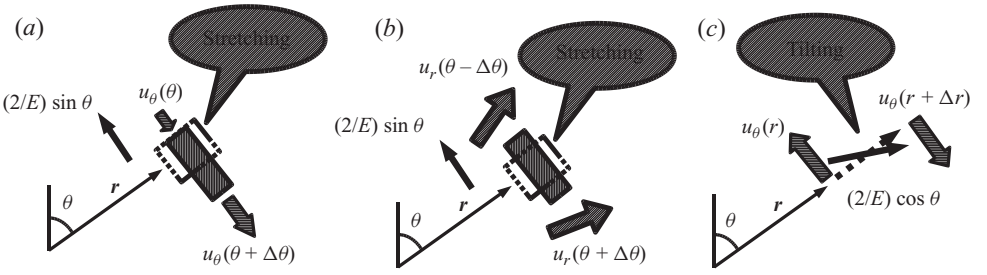

FIGURE 4. Physical meanings of the terms in the equation of the colatitudinal component of vorticity given by (4.1). (*a*) Stretching and shrinking of the colatitudinal component of planetary vorticity by the divergence and convergence of the colatitudinal component of velocity, $-(2/E)(\sin\theta/r)(\partial u_\theta/\partial\theta)$. (*b*) Stretching and shrinking of the colatitudinal component of planetary vorticity by the radial component of velocity, $-(2/E)(u_r \sin\theta/r)$. (*c*) Tilting of the radial component of planetary vorticity by the radial shear of the colatitudinal component of velocity, $(2/E)\cos\theta(\partial u_\theta/\partial r)$.

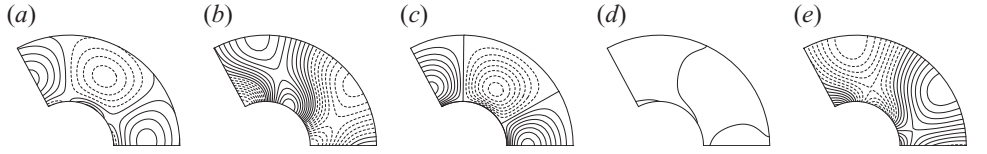

FIGURE 5. Distribution of each term in the equation of the colatitudinal component of vorticity given by (4.1) for the critical thermal convection in the slowly rotating spherical shell shown in figure 1. The equatorial cross-sections are shown. Only the regions between the azimuthal angles of 0° and 120° are presented, because the azimuthal wavenumber of the solution is three. Solid and broken contour lines indicate positive and negative values, respectively. (*a*) Temporal variation of the colatitudinal component of vorticity, $\partial\omega_\theta/\partial t$. (*b*) Stretching and shrinking of the colatitudinal component of planetary vorticity by the divergence and convergence of the colatitudinal component of velocity, $-(2/E)(\sin\theta/r)(\partial u_\theta/\partial\theta)$. (*c*) Stretching and shrinking of the colatitudinal component of planetary vorticity by the radial component of velocity, $-(2/E)(u_r \sin\theta/r)$. (*d*) Tilting of the radial component of planetary vorticity by the radial shear of the colatitudinal component of velocity, $(2/E)\cos\theta(\partial u_\theta/\partial r)$. This term is exactly zero on the equatorial plane. (*e*) Generation by the azimuthal temperature gradient and the viscous dissipation of the colatitudinal component of vorticity.

where ϕ and θ denote azimuth and colatitude, respectively. Here, $\nabla\times\boldsymbol{u}=\boldsymbol{\omega}=(\omega_r, \omega_\theta, \omega_\phi)$ and $\boldsymbol{u}=(u_r, u_\theta, u_\phi)$ are the vorticity and velocity components, respectively. The first and second terms, which are proportional to $(2/E)$ in the right-hand side of (4.1), denote the variation of the colatitudinal component of relative vorticity through stretching and shrinking the colatitudinal component of planetary vorticity (figures 4*a* and 4*b*). The third term, which is proportional to $(2/E)$, indicates that the colatitudinal component of relative vorticity varies through tilting of the radial component of planetary vorticity by the radial shear of the colatitudinal velocity (figure 4*c*). The term that is proportional to the temperature gradient in the right-hand side of (4.1) represents the generation of vorticity by the buoyancy force, and the final terms represent the viscous dissipation of vorticity.

Figure 5 shows the distribution on the equatorial cross-section of each term in the equation of the colatitudinal component of vorticity given by (4.1) for the critical thermal convection in the slowly rotating spherical shell presented in figure 1. In the right-hand side of (4.1), the dominant term is $-(2/E)(\sin\theta/r)(\partial u_\theta/\partial\theta)$ (figure 5*b*). However, the distribution of the dominant term is not consistent with

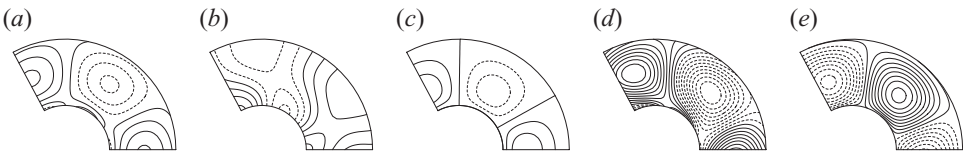

FIGURE 6. Distribution of each term in the equation of the colatitudinal component of vorticity given by (4.1) for the critical thermal convection in the slowly rotating spherical shell shown in figure 1. The conical surfaces at 45° colatitude are shown. Only the regions between azimuthal angles of 0° and 120° are presented, because the azimuthal wavenumber of the solution is three. Solid and broken contour lines indicate positive and negative values, respectively. (*a*) $\partial\omega_\theta/\partial t$. (*b*) $-(2/E)(\sin\theta/r)(\partial u_\theta/\partial\theta)$. (*c*) $-(2/E)(u_r\sin\theta/r)$. (*d*) $(2/E)\cos\theta(\partial u_\theta/\partial r)$. (*e*) Generation by the azimuthal temperature gradient and the viscous dissipation of the colatitudinal component of vorticity.

the temporal variation of the colatitudinal component of vorticity (figure 5*a*). This term is exactly balanced by the vorticity generation and dissipation terms (figure 5*e*). Here, $(2/E)\cos\theta(\partial u_\theta/\partial r)$ does not contribute to $\partial\omega_\theta/\partial t$ because the radial component of planetary vorticity vanishes on the equatorial plane (figure 5*d*). As a result, $-(2/E)(u_r\sin\theta/r)$ governs the temporal variation of colatitudinal vorticity (figure 5*c*). Therefore, it can be concluded that, in the equatorial region, the retrograde propagation is caused by stretching and shrinking of the colatitudinal component of planetary vorticity by the radial component of velocity.

On the other hand, figure 6 shows the distribution on the conical surface at 45° colatitude of each term in (4.1) for the same critical thermal convection. In the right-hand side of (4.1), the dominant term is $(2/E)\cos\theta(\partial u_\theta/\partial r)$ (figure 6*d*), the distribution of which is consistent with $\partial\omega_\theta/\partial t$ (figure 6*a*). This distribution is weakened by the vorticity generation and dissipation terms (figure 6*e*) and the temporal variation of the colatitudinal component of vorticity shown in figure 6(*a*) is produced. The contribution of $-(2/E)(\sin\theta/r)(\partial u_\theta/\partial\theta)$ and $-(2/E)(u_r\sin\theta/r)$ is relatively small at mid-latitudes (figures 6*b* and 6*c*). Therefore, in contrast to the equatorial region, the retrograde propagation is caused by tilting of the radial component of planetary vorticity by the radial shear of the colatitudinal component of velocity at mid-latitudes.

Figure 7 compares the magnitude of each term in the equation of the colatitudinal component of vorticity given by (4.1) at $E=0.1$ and $\eta=0.4$ for various values of the Prandtl number. The colatitudinal distributions of the terms are plotted at the azimuthal and radial positions, where the temporal variation of the colatitudinal component of vorticity becomes maximum on the equatorial plane.

Based on figure 7(*b*), we can confirm the tendency of the vorticity budget mentioned above in the case of the Prandtl number $P=1$. From the equator to the 60° colatitude, $-(2/E)(u_r\sin\theta/r)$ (short-dashed line) largely contributes to the temporal variation of the colatitudinal component of vorticity (solid line), whereas at latitudes higher than 60° colatitude, the contribution of $(2/E)\cos\theta(\partial u_\theta/\partial r)$ (long dashed-dotted line) becomes larger. The term of the generation by the azimuthal temperature gradient and by the viscous dissipation of the colatitudinal component of vorticity (long dashed double-dotted line) cancels these terms of the vorticity budget to a certain extent.

Based on figures 7(*a*) and 7(*c*), the tendency of relative amplitude of the terms of $-(2/E)(u_r\sin\theta/r)$ (short-dashed line) and $(2/E)\cos\theta(\partial u_\theta/\partial r)$ (long dashed-dotted line) does not change, even when the Prandtl number is varied, namely,

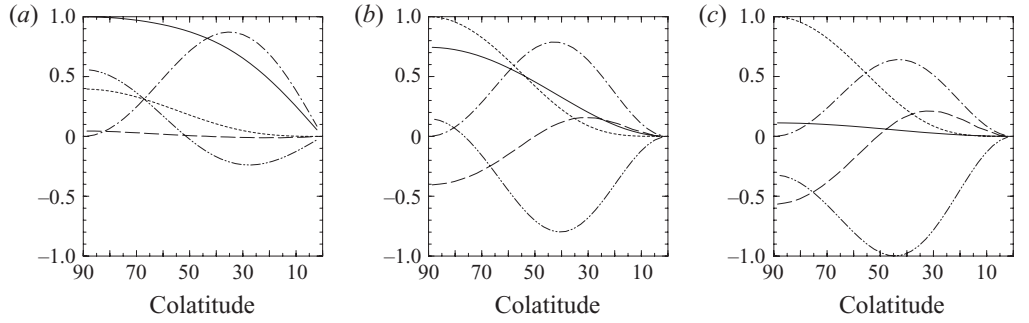

FIGURE 7. The comparison of each term in the equation of the colatitudinal component of vorticity given by (4.1) of the critical thermal convection in a slowly rotating spherical shell at $E=0.1$ and $\eta=0.4$ for various values of the Prandtl number. The colatitudinal distribution of each term is shown at the azimuthal and radial positions, where the temporal variation of the colatitudinal component of vorticity becomes maximum on the equatorial plane. The range of the colatitude $0^\circ \leqslant \theta \leqslant 90^\circ$ is plotted because all of the terms of the vorticity budget are equatorially symmetric: (*a*) $P=0.1$, (*b*) $P=1$ and (*c*) $P=10$. The solid, long-dashed, short-dashed, long dashed dotted, and long dashed double-dotted lines indicate $\partial\omega_\theta/\partial t$, $-(2/E)(\sin\theta/r)(\partial u_\theta/\partial\theta)$, $-(2/E)(u_r\sin\theta/r)$, $(2/E)\cos\theta(\partial u_\theta/\partial r)$, and generation by the azimuthal temperature gradient and the viscous dissipation of the colatitudinal component of vorticity, respectively. The values are normalized with the amplitude of the largest term at the equator.

$-(2/E)(u_r\sin\theta/r)$ is larger than $(2/E)\cos\theta(\partial u_\theta/\partial r)$ in the equatorial region, whereas $(2/E)\cos\theta(\partial u_\theta/\partial r)$ is dominant at mid-latitudes. However, the relative magnitude of the term of generation and viscous dissipation of the colatitudinal component of vorticity (long dashed double-dotted line) around the equator changes according to the Prandtl number. When the Prandtl number becomes large, it cancels the term of $-(2/E)(u_r\sin\theta/r)$ (short-dashed line) and reduces the temporal variation of colatitudinal component of vorticity (solid line). On the other hand, when the Prandtl number is decreased, it enhances the term of $-(2/E)(u_r\sin\theta/r)$ (short-dashed line) and increases the temporal variation of the colatitudinal component of vorticity (solid line).

The balance between the vorticity budget terms described above does not change in the range of the Ekman number $10 \geqslant E \geqslant 10^{-1}$. When the radius ratio is increased up to $\eta=0.8$, critical convection with the Y_l^l type horizontal structure still emerges, but the horizontal total wavenumber l is increased. The latitudinal extent of critical convection then becomes smaller, and the colatitudinal distribution of each term of the vorticity budget concentrates around the equatorial region. However, the tendency of the balance between the vorticity budget terms is unchanged.

The preliminary analysis also shows that the balance of the vorticity budget terms remains unchanged, even when the heating mode is changed by internal heating to radial differential heating. However, for the case of the imposed heat flux condition instead of the fixed temperature condition, it is difficult to identify the dominant term that is responsible for the retrograde propagation due to the smallness of the temporal variation of the colatitudinal component of vorticity. The balance of vorticity budget terms for the imposed heat flux cases appears to differ from that for the fixed-temperature cases, possibly because the horizontal structure of critical convection is extended in the azimuthal direction and a Y_1^1 type structure emerges under the imposed heat flux condition.

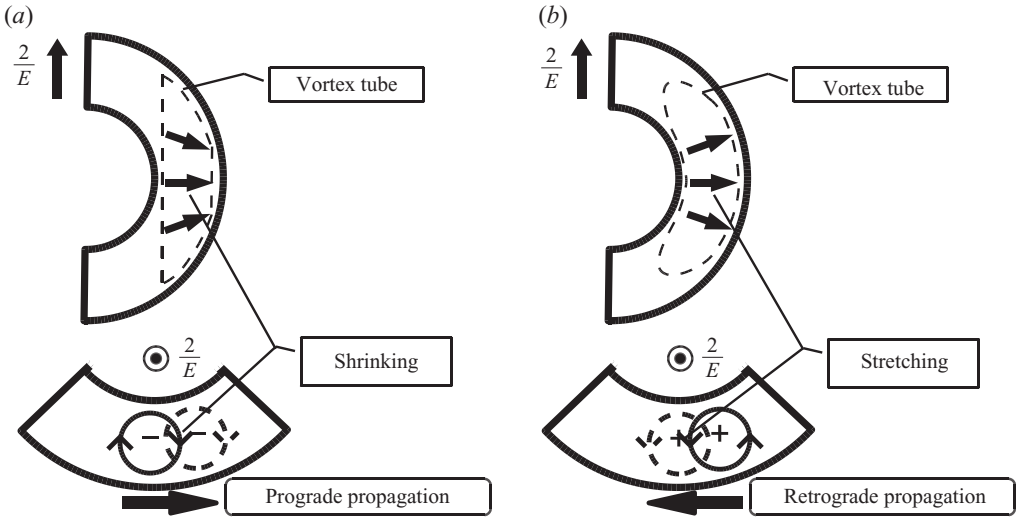

FIGURE 8. Schematic diagrams of the propagation mechanism of vortices. (*a*) Rapidly rotating case. The vortices propagate in the prograde direction due to shrinking of the fluid columns accompanied by cylindrical-radially outward flows. (*b*) Slowly rotating case. The vortices propagate in the retrograde direction due to stretching of the fluid columns accompanied by cylindrical-radially outward flows.

5. Summary

We have investigated the retrograde propagation mechanism of critical thermal convection with a sectorial pattern emerging in a slowly rotating spherical shell through a vorticity budget analysis. It is revealed that the propagation mechanism changes depending on the colatitudinal position. In the equatorial region, retrograde propagation is caused by stretching and shrinking of the colatitudinal component of planetary vorticity by the radial component of velocity, whereas at mid-latitudes, retrograde propagation is caused by tilting of the radial component of planetary vorticity by the radial shear of the colatitudinal component of velocity. The term of generation and viscous dissipation of the colatitudinal component of vorticity enhances or reduces these terms to a certain extent depending on the Prandtl number.

We can understand the switching mechanism of the propagating direction between slowly and rapidly rotation cases by focusing on the vorticity generation around the equatorial region. The prograde propagation of vortex columns in rapidly rotating cases can be explained by the topographic β effect of the outer spherical boundary, which causes shrinking (stretching) of the fluid columns accompanied by their cylindrical-radially outward (inward) movement. Due to the conservation of potential vorticity, when fluid columns are shrunk, they must rotate more slowly than the shell, thereby inducing negative relative vorticity. On the other hand, when fluid columns are stretched, they must rotate faster than the shell, inducing positive relative vorticity. Since positive vorticity columns accompany inward flows on the prograde side, they propagate in the prograde direction (figure 8*a*). The tendency of stretching and shrinking of the fluid columns can be confirmed in the meridional cross-section shown in figure 2(*b*). The velocity field converges in the direction of the axis of rotation associated with the cylindrical-radially outward component.

On the other hand, in slowly rotating cases, the vorticity budget analysis performed in §4 revealed that stretching and shrinking of the colatitudinal component of planetary vorticity by the radial component of velocity governs the retrograde propagation around the equatorial region. Note that the outward radial component of velocity causes cylindrical-radially outward movement and stretching of the fluid columns at the same time. The meridional cross-section of the convection structure in the slowly rotating case shown in figure 1(*b*) reveals that stretching of the fluid columns occurs concurrently with their cylindrical-radially outward movement. The correlation between the stretching/shrinking and outward/inward flows is opposite to that in the rapidly rotating case, which contributes to the retrograde propagation (figure 8*b*).

The difference in the stretching/shrinking tendency originated from the different alignment direction of the vortex tubes. When the effect of the rotation of the shell is strong, vortex tubes are elongated along the axis of rotation according to the Taylor–Proudman constraint. The convergence in the axial direction associated with the outward fluid motion is due to the distortion of Taylor vortex columns by the outer spherical surface. On the other hand, when the effect of the rotation of the shell is sufficiently weak, the vortex tubes tend to be elongated along the spherical shell and bent into a banana-shaped form. Therefore, divergence in the axial direction associated with the cylindrical-radially outward fluid motion is induced.

The numerical calculations were performed by the computer systems of the Institute for Information Management and Communication (IIMC) of Kyoto University. For the calculation of the critical modes of convection, the library for spectral transform ISPACK (http://www.gfd-dennou.org/library/ispack/) and its Fortran90 wrapper library SPMODEL library (Takehiro *et al.* 2006) were used. The eigenvalue problems were solved using the subroutine of the Fujitsu SSL II library. The products of the Dennou Ruby project (http://www.gfd-dennou.org/library/ruby/) were used to draw the figures.

REFERENCES

Busse, F. H. 1970*a* Differential rotation in stellar convection zones. *Astrophys. J.* **159**, 629–639.

Busse, F. H. 1970*b* Thermal instabilities in rapidly rotating systems. *J. Fluid Mech.* **44**, 441–460.

Busse, F. H. 1973 Differential rotation in stellar convection zones. Part II. *Astron. Astrophys.* **28**, 27–37.

Busse, F. H. 1986 Asymptotic theory of convection in a rotating, cylindrical annulus. *J. Fluid Mech.* **173**, 545–556.

Chandrasekhar, S. 1961 *Hydrodynamic and Hdromagnetic Stability*. Oxford University Press, 652 pp.

Dormy, E., Soward, A. M., Jones, C. A., Jault, D. & Cardin, P. 2003 The onset of thermal convection in rotating spherical shells. *J. Fluid Mech.* **501**, 43–70.

Geiger, G. & Busse, F. H. 1981 On the onset of thermal convection in slowly rotating fluid shells. *Geophys. Astrophys. Fluid Dyn.* **18**, 147–156.

Gilman, P. A. 1975 Linear simulations of Boussinesq convection in a deep rotating spherical shell. *J. Atmos. Sci.* **32**, 1331–1352.

Hirsching, W. R. & Yano, J.-I. 1994 Metamorphosis of marginal thermal convection in rapidly rotating self-gravitating spherical shells. *Geophys. Astrophys. Fluid Dyn.* **74**, 143–179.

Jones, C. A., Soward, A. M. & Mussa, A. I. 2000 The onset of thermal convection in a rapidly rotating sphere. *J. Fluid Mech.* **405**, 157–179.

Roberts, P. H. 1968 On the thermal instability of a rotating-fluid sphere containing heat sources. *Phil. Trans. R. Soc. Lond.* **A163**, 93–117.

Takehiro, S. 2008 Physical interpretation of spiralling-columnar convection in a rapidly rotating annulus with radial propagation properties of Rossby waves. *J. Fluid Mech.* **614**, 67–86.

Takehiro, S. & Hayashi, Y.-Y. 1995 Boussinesq convection in rotating spherical shells – a study on the equatorial superrotation. In *The Earth's Central Part: Its Structure and Dymamics* (ed. T. Yukutake), pp. 123–156, TERAPUB.

Takehiro, S., Odaka, M., Ishioka, K., Ishiwatari, M., Hayashi, Y.-Y. & SPMODEL Development Group 2006 A series of hierarchical spectral models for geophyiscal fluid dynamics. *Nagare Multimedia 2006*, http://www.nagare.or.jp/mm/2006/spmodel/.

Yano, J.-I. 1992 Asymptotic theory of thermal convection in rapidly rotating systems. *J. Fluid Mech.* **243**, 103–131.

Zhang, K. 1992 Spiralling columnar convection in rapidly rotating spherical fluid shells. *J. Fluid Mech.* **236**, 535–556.

Zhang, K. 1993 On equatorially trapped boundary inertial waves. *J. Fluid Mech.* **248**, 203–217.

Zhang, K. 1994 On coupling between the Poincare equation and the heat equation. *J. Fluid Mech.* **268**, 211–229.

Zhang, K.-K. & Busse, F. H. 1987 On the onset of convection in rotating spherical shells. *Geophys. Astrophys. Fluid Dyn.* **39**, 119–147.